HCHO oxidation on Pt-Na/SiO₂ catalyst with ultralow Pt loading: New insight into the effect of Si support and Na promoter

Jingyi Wang [a,d], Guangzhi He [c], Chunying Wang [a,b], Xudong Chen [a,d], Xiaofeng Liu [e], Yaobin Li [a,b,*], Wenpo Shan [a,b], Hong He [a,b,c,d,*]

[a] Center for Excellence in Regional Atmospheric Environment, Key Laboratory of Urban Pollutant Conversion, Institute of Urban Environment, Chinese Academy of Sciences, Xiamen 361021, China
[b] Zhejiang Key Laboratory of Urban Environmental Processes and Pollution Control, CAS Haixi Industrial Technology Innovation Center in Beilun, Ningbo 315800, China
[c] State Key Joint Laboratory of Environment Simulation and Pollution Control, Research Center for Eco-environmental Sciences, Chinese Academy of Sciences, Beijing 100085, China
[d] University of Chinese Academy of Sciences, Beijing 100049, China
[e] School of Resources & Chemical Engineering, Sanming University, Sanming 365004, China

ARTICLE INFO

ABSTRACT

Modulating the electronic metal-support interaction (EMSI) is one of the effective means to promote catalytic activity because it can adjust the electron occupancy of the *d*-band of noble metals, further facilitating the activation of reactants. Herein, we prepared a Pt/SiO₂ catalyst with an ultralow Pt loading of 0.05% and found that its catalytic activity in HCHO oxidation outperformed that of the Pt/TiO₂ counterpart, owing to the EMSI effect between Pt and SiO₂. On this basis, the alkali metal Na was used as a promoter, and the formation of highly active Pt-O$_x$(OH)-Na clusters enabled the complete oxidation of HCHO at room temperature. With ultralow Pt loading, the Pt-Na/SiO₂ catalyst reduces the cost of practical application remarkably. *In situ* DRIFTS and DFT calculations confirmed that the reaction pathways were distinct on Pt/SiO₂ and Pt-Na/SiO₂. Specifically, on Pt-Na/SiO₂, the reaction follows the mechanism of the direct degradation of formate species with the assistance of active hydroxyls; while on Pt/SiO₂, CO is the only intermediate formed by the dehydrogenation of HCHO, due to the lack of active hydroxyls. These findings provide new insights into the reaction pathway of HCHO oxidation.

1. Introduction

Formaldehyde, as one of the prevalent indoor air contaminants, is highly detrimental to human health even at very low concentration [1–3]. It was classified as a Group I carcinogen, and the maximum indoor concentration of HCHO should not exceed 0.1 mg/m³, according to the guidelines of the International Agency for Research on Cancer (IRAC). Long-term exposure to HCHO can lead to respiratory diseases, pneumonia and eventually cancer [4]. Hence, various approaches have been developed for indoor HCHO removal, among which heterogeneous catalysis stands out for being energy-efficient and environmentally friendly [5–7]. Among all catalysts, platinum-based catalysts are of prime concern for their efficiency [8]. However, the usage of platinum group metals (PGMs) is severely limited by the high cost of noble metals; hence, it is of great importance to lower the cost through the modification of supports and/or use of promoters [9,10].

Essentially, the activity of PGMs catalysts is modulated by the nature of the supports. For instance, on reducible supports like TiO₂ and CeO₂, manipulating oxygen vacancies and further promoting strong metal-support interactions (SMSI) via H₂ reduction is a prominent strategy [11–15], for the SMSI effect can modulate the electron distribution of the *d*-band of PGMs, and further influence their abilities for adsorbing and activating molecules like O₂ [16]. In contrast, the SMSI has difficulty occurring on irreducible supports (such as Al₂O₃, SiO₂, zeolites, etc.). Nevertheless, PGMs supported on irreducible supports like Al₂O₃, activated carbon (AC) and zeolites still present extraordinary ability for oxidizing HCHO, due to the presence of sufficient OH species, the anchoring effect for PGMs, special micropore structures, etc. [17–20]. Silica, with good thermal and mechanical stability, as well as abundant OH and tunable porosity, is one of the most commonly used supports for

PGMs [21]. Therefore, we inferred that SiO_2 might be an applicable support as well for PGMs.

As aforementioned, the typical SMSI is hard to form on M/SiO_2 (M stands for PGMs). However, according to Pauling scale, the electronegativity of Si is lower than that of PGMs, Si would act as an electron donor and PGMs would carry negative charges [22]. This phenomenon could be classified as an electronic metal-support interaction (EMSI). Zheng et al. have prepared Si-doped TiO_2 as the support of Pt and found that Si doping generated more $Pt^{\delta-}$ species [23]. Meanwhile, Jimenez-Izal has used Pt_2X/MgO (X = B, Si, Sn, Al, etc.) as the model catalyst to analyze the electronic flows, and found that Si exhibited the best potential electron donor ability among the above promoters [24]. Additionally, it should be noted that PGMs can directly bond to Si without O-bridge. This unique feature has made it possible for the synthesis of intermetallic silicides composed of Si and PGMs (IrSi, PtSi, RhSi, etc.), and it has been verified that Si modulates the *d*-band center of PGMs and further influences their catalytic activity [25]. Moreover, through building an SiO_2 overlayer on Pd/ZSM-5 catalyst (Pd@SiO_2/ZSM-5), Pd-Si bonding had been observed through EXAFS, which firmly proved the existence of the interface between PGMs and silica [26].

The addition of promoters can improve the performance of catalysts, and alkali metals are one of the most used promoters in the water-gas shift reaction (WGS), NO_x storage and reduction (NSR), HCHO oxidation, etc. [10,27–32]. With the addition of alkali metals, the dispersion of PGMs is greatly promoted, leading to better catalytic activity [33]. Additionally, as alkali metals have the lowest electronegativities, the electrons of alkali metals would naturally flow to PGMs and form electron-rich PGMs, which would enhance O_2 adsorption and activation [32]. Moreover, Zhang et al. proved that the highly active species noble metal-alkali-O_x-$(OH)_y$ could change the reaction pathway because of the participation of active OH [10]. In previous research on Pt-Na/TiO_2 and Pt-Na/Al_2O_3, the noble metal-alkali-O_x-$(OH)_y$ species was proven to be atomically dispersed [17]. However, since the inert SiO_2 support lacks anchoring sites, like oxygen vacancies on TiO_2 or Al_{penta} on γ-Al_2O_3 [34], the form and nature of Pt-O_x(OH)-Na on SiO_2 is worth exploration.

In this work, we have prepared Pt/SiO_2 and Pt-Na/SiO_2 catalysts with an ultralow Pt loading of 0.05 wt%, and for comparison, Pt/TiO_2 was also prepared and tested. Notably, the performance of Pt/SiO_2 is far beyond that of Pt/TiO_2, and Na addition further enhances the activity of Pt/SiO_2 catalyst for HCHO oxidation at ambient temperature. Based on the results of characterization and calculations, the effects of SiO_2 and Na on the performance and reaction pathway of HCHO catalytic oxidation on Pt/SiO_2 catalyst were clarified, which is of great value in practical application.

2. Experimental section

2.1. Materials preparation

Pt/SiO_2, Pt-Na/SiO_2 and Pt/TiO_2 catalysts were prepared by the impregnation method, using $Pt(NO_3)_2$ (Heraeus) as the Pt precursor and Na_2CO_3 (Sinopharm) as the Na precursor. The SiO_2 and TiO_2 supports were purchased from Aladdin. The theoretical Pt and Na loadings were 0.05 wt% and 0.20 wt%, respectively. After impregnation under stirring for 3 h, excess water was removed by rotary evaporation at 60 °C. Afterward, the samples were dried at 110 °C overnight, followed by calcination at 400 °C in muffle ovens. It is worth noting that reduction in 10% H_2/N_2 at 300 °C for 1 h is a prerequisite before any activity testing or characterization.

2.2. Catalyst characterization and DFT calculation details

Catalyst characterization and DFT calculation details are described in Supporting Information.

2.3. Activity test for HCHO oxidation

The catalytic activity test for HCHO oxidation was performed in a fixed-bed quartz reactor (d = 4 mm) in an incubator kept at 25 °C. Gaseous HCHO was generated by bubbling He through para-formaldehyde, and the relative humidity (RH) was maintained by passing He through a water bubbler to generate water vapor. The fed gas was composed of 120 ppm HCHO, 20% O_2 and 35% RH balanced by He.

In the activity test, the total flow rate was kept at 100 mL/min, and the corresponding weight hourly space velocity (WHSV) was kept at 200,000 mL/(g_{cat}·h) for the Pt/SiO_2 and Pt-Na/SiO_2 catalysts, and 60,000 mL/(g_{cat}·h) for the Pt/TiO_2 catalyst. The inlet and outlet gas were monitored by an FTIR spectrometer (Nicolet iS50) equipped with a DGTS detector (resolution: 0.5 cm^{-1}, collect range: 4000–400 cm^{-1}). In all experiments, HCHO conversion (%) was calculated by:

$$HCHO \quad conversion \quad (\%) = \left(1 - \frac{[HCHO]_{in}}{[HCHO]_{out}} \right) \times 100\%$$

And CO_2 yield (%) was calculated by:

$$CO_2 \quad yield \quad (\%) = \frac{[CO_2]}{[HCHO]_{in}} \times 100\%$$

where the $[HCHO]_{in}$ and $[HCHO]_{out}$ refer to the concentration of HCHO in the inlet and outlet gas, and $[CO_2]$ represents the concentration of CO_2 in the outlet gas.

The equation used for the calculation of turnover frequency (TOF, s^{-1}) is displayed in the Supporting Information.

3. Results

3.1. Activity test

The catalytic performance of the Pt/SiO_2 and Pt-Na/SiO_2 catalysts at ambient temperature was evaluated and presented in Fig. 1. For Pt/SiO_2, 30% HCHO conversion was achieved for 6 h, with the corresponding CO_2 yield, while for the contrasting sample of Pt/TiO_2, the constant CO_2 yield was less than 5% over 6 h. It is intriguing that with an ultralow Pt loading of 0.05%, the Pt/SiO_2 catalyst possessed better HCHO oxidation performance than the Pt/TiO_2 catalyst. With the addition of Na, the HCHO conversion of the Pt/SiO_2 catalyst was further enhanced greatly and maintained at 100% for 6 h.

Based on the Pt dispersion (Table 1), the turnover frequency (TOF) at 25 °C was calculated and the results are demonstrated in Table 1. The TOF values for Pt/TiO_2, Pt/SiO_2 and Pt-Na/SiO_2 were 2.66×10^{-3}, 8.74×10^{-2} and 2.69×10^{-1} s^{-1}, respectively. It is clear that the use of SiO_2 as support and Na as promoter enhanced the intrinsic activity of the Pt-based catalysts, and led to better capability in HCHO oxidation at room temperature.

3.2. Structural features

The XRD patterns of catalysts and supports are shown in Fig. S1. There were no diffraction peaks corresponding to Pt observed for the Pt/TiO_2, Pt/SiO_2 and Pt-Na/SiO_2 catalysts, suggesting that Pt was well-dispersed. The specific area and pore size distribution of catalysts and supports were measured by nitrogen adsorption-desorption isotherms, and the results are shown in Table 1 and Table S1. There were no significant differences in specific area between the catalysts and corresponding supports.

3.3. Effect of the SiO_2 support

As mentioned above, the catalytic activity of Pt/SiO_2 was far better than that of Pt/TiO_2. Since TiO_2 and SiO_2 had no catalytic activity for HCHO oxidation, we will mainly focus on their impact on Pt. According
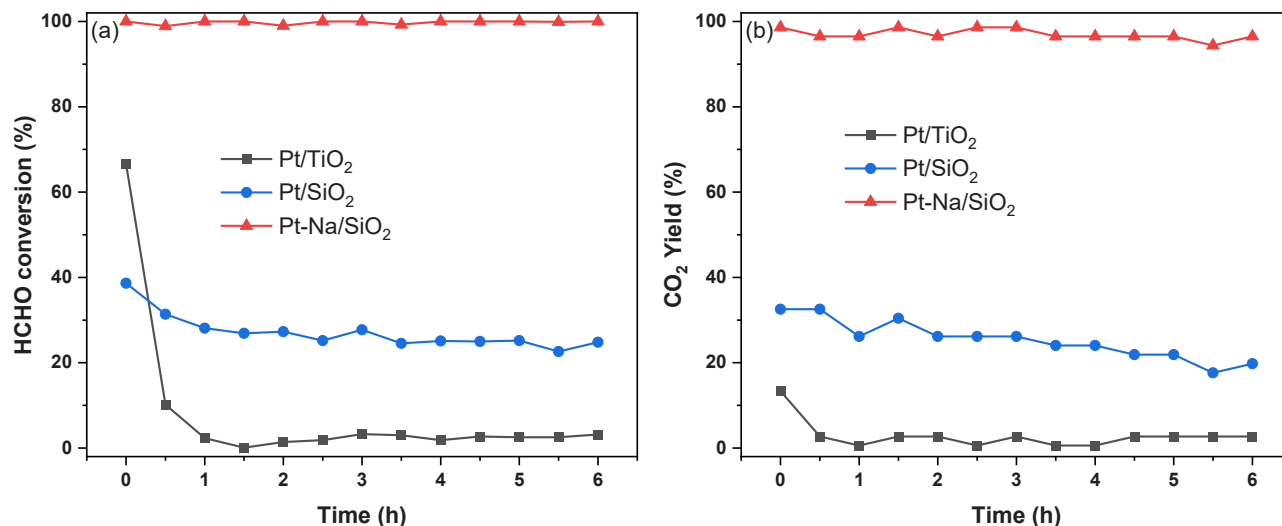
Fig. 1. (a) HCHO conversion and (b) CO_2 yield on Pt/TiO_2, Pt/SiO_2 and $Pt-Na/SiO_2$ catalysts at 25 °C. Reaction conditions: 120 ppm HCHO, 35% RH, 20% O_2, He balance, WHSV of 200,000 mL/(g_{cat}·h) for Pt/SiO_2 and $Pt-Na/SiO_2$ and 60,000 mL/(g_{cat}·h) for Pt/TiO_2 catalyst.

Table 1
Specific Surface Area (BET), Total Pore Volume, Pore size, Pt dispersion and TOF of Pt/SiO_2, $Pt-Na/SiO_2$ and Pt/TiO_2.

Samples	S_{BET} (m^2/g)	V_{pore} (cm^3/g)	Pore size (nm)	D_{co}[a] (%)	TOF[b] (s^{-1})	d_M[c] (nm)
Pt/SiO_2	144.17	1.03	29.53	47.58	8.74×10^{-2}	1.55
$Pt-Na/SiO_2$	132.32	1.00	30.51	94.50	2.69×10^{-1}	1.23
Pt/TiO_2	73.34	0.36	17.26	84.94	2.66×10^{-3}	-

[a] Pt dispersion based on CO pulse chemisorption.
[b] Turnover frequencies (TOF) based on D_{CO}.
[c] Pt particle distribution measured by HAADF-STEM.

to the previous works, Si could adjust the electron distribution between Si and PGMs [24,25]; hence, DFT calculations were applied to analyze electron flows at the Pt-SiO_2 interfaces.

As shown in Fig. S2, after attaching the Pt_4 cluster to the SiO_2 slab, reconstruction of the surface of SiO_2 occurred at the interface, which led to direct bonding between Pt and Si, while this phenomenon was not observed at the Pt_4-TiO_2 interface. According to the literature, Si could modulate the *d*-band center of PGMs [25,26]; hence, the calculated partial density of states of the Pt-*d* orbitals in Pt/SiO_2 and Pt/TiO_2 are shown in Fig. 2a, b. It can be found that the *d*-band center (ε_d) of Pt/TiO_2 (−2.12 eV) is similar to that of metallic Pt (−2.25 eV), while the ε_d of Pt/SiO_2 (−1.48 eV) moves closer to the Fermi level. According to previous research, the ε_d of PGMs determines their adsorption and activation ability for O_2; that is, specifically, the higher ε_d metals have, the stronger the interaction between the metals and O_2, leading to easier activation of O_2 [16,26,35]. Hence, with the ε_d of Pt increasing, the ability of Pt/SiO_2 for O_2 activation was enhanced, which further improved its performance of HCHO oxidation. Fig. 2c-d shows the differential charge density on Pt/TiO_2 and Pt/SiO_2, with the corresponding planar average in the z-direction. As seen in the figure, the contact between Pt and the supports results in charge redistribution at the interfaces. According to Bader charge analysis, 0.28 e⁻ of electrons transferred from Pt to the TiO_2 support on the Pt/TiO_2 catalyst. Interestingly, different from the Pt/TiO_2 catalyst, the direction of electron transfer on the Pt/SiO_2 catalyst was inverse; that is, 1.54 e⁻ of electrons transferred from the SiO_2 support to Pt, which leads to the accumulation of electrons around Pt atoms at Pt-SiO_2 interfaces. Furthermore, the electron density of the second layer of Pt_4 on the Pt/SiO_2 catalyst (0.10 e/Å) was higher than that on the Pt/SiO_2 catalyst (0.03 e/Å), which was ascribed to the EMSI between Pt and SiO_2 or TiO_2. It is well

known that the negatively charged Pt could increase the electron donation from the *d*-band to the antibonding π^* orbital of O_2, and consequently enhance the activation of O_2 [36,37]. As depicted in Fig. S3, Pt/TiO_2 and Pt/SiO_2 with adsorbed O_2 molecules were optimized, and the corresponding adsorption energies were − 1.10 eV and − 2.71 eV, respectively. The distance between O atoms were measured, as the descriptor for the extent of O_2 activation. The bond length of O_2 molecule is 1.21 Å, while on Pt/TiO_2 and Pt/SiO_2, the bond was elongated to 1.29 Å and 1.45 Å, respectively. The latter should be classified as superoxide species (O_2^-*, $d_{(O-O)} = 1.35$ Å), which is highly active in catalytic reactions. In conclusion, Pt on the SiO_2 support, with higher *d*-band center and more electrons accumulated, would exhibit better HCHO oxidation performance than the Pt/TiO_2 catalyst.

To further confirm the phenomenon, XPS measurements were conducted on Pt/SiO_2 and Pt/TiO_2 samples with 0.20% Pt loading, and the result is shown in Fig. S4. The peaks at 70.9 eV and 71.3 eV were assigned to Pt^0, and the peaks at 73.0 eV and 74.1 eV were ascribed to Pt of higher valence state ($Pt^{\delta+}$, δ = 2–4) [38]. Compared to Pt/TiO_2, the binding energy of Pt^0 on Pt/SiO_2 shifted to lower energy and the proportion of Pt^0 species was higher, which corresponded well to the calculation results.

3.4. The effect of Na promoter

3.4.1. Charge distribution analysis

Alkali metals are well known as electron donors, and based on the Pt/SiO_2 catalyst, we further analyzed the impact of Na from the prospective of the charge distribution. After adding a Na atom to the model of Pt/SiO_2, the number of electrons transferred increased to 1.90 e⁻ (Fig. 2e), and the influence from SiO_2 to the second layer of Pt_4 increased to 0.16 e/Å, suggesting the existence of strong interaction between alkalis and noble metals. However, the ε_d of the Pt was similar to that of the Pt/SiO_2 catalyst (Fig. S5, $\varepsilon_d = -1.52$ eV). Therefore, from the prospective of charge distribution, it was concluded that the influence of the Na promoter mostly focused on donating charges to Pt, while the impact of the SiO_2 support involved two aspects, including modulation of the *d*-band charge occupancy of Pt, and the EMSI, which induced the charge accumulation on Pt.

3.4.2. State of Pt species

The particle size of Pt was observed and measured by HAADF-STEM, and the results are shown in Fig. 3. According to Figs. 3a and 3c, the mean particle size on Pt/SiO_2 and $Pt-Na/SiO_2$ was 1.56 nm and 1.23 nm,
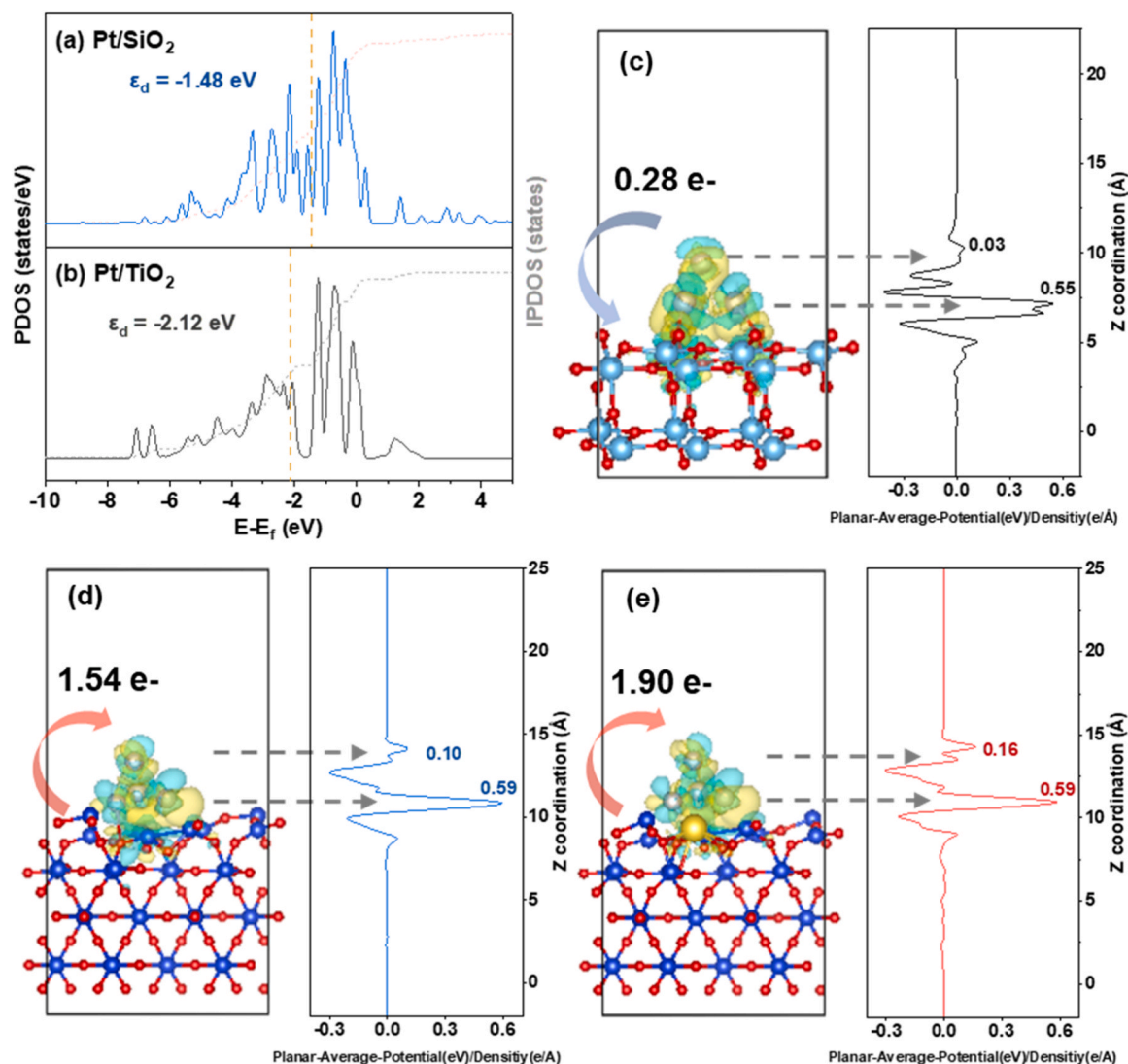
Fig. 2. PDOS of Pt-d orbital in (a) Pt/SiO$_2$ and (b) Pt/TiO$_2$; the side views of the optimized structures with differential charge density and the corresponding planar average in z-direction of (c) Pt/TiO$_2$, (d) Pt/SiO$_2$, and (e) Pt-Na/SiO$_2$. Red, blue, grey, navy, yellow balls denote as O, Ti, Pt, Si and Na, respectively. Yellow in charge distribution refers to accumulation and blue refers to depletion.

respectively. The results of Pt particle sizes of catalysts based on volume average are shown in Table S2. In addition, the Pt dispersion was examined by CO chemisorption, and was 47.58% for Pt/SiO$_2$ and 94.50% for Pt-Na/SiO$_2$. It is intriguing that the Pt dispersion of Pt-Na/SiO$_2$ was extraordinary, reaching almost atomical dispersion; however, this was not consistent to the Pt particle size observed by STEM. According to the previous work, the addition of alkali metal could stabilize atomically dispersed Pt, and generate the highly active species of Pt-O$_x$(OH)-Na [10]. Nevertheless, in this case, during the reduction process at 300 ℃ before testing, Pt or Pt-O$_x$(OH)-Na species tended to aggregate to form Pt particles and clusters on Pt/SiO$_2$ or Pt-Na/SiO$_2$ catalysts As shown in Fig. 3b, without Na addition, Pt formed solid nanoparticles, where the lattice fringe of Pt(110) could be observed explicitly. This indicates that Pt atoms have a strong tendency of agglomeration and crystallization in reducing atmosphere. A considerable amount of Pt could not be exposed to the surface in the Pt particle; as we speculated, at most 56% of Pt emerged at the surface in the truncated octahedron model of a Pt particle of 1.5 nm (inset of Fig. 3b). By contrast, as shown in Fig. 3d, after Na doping, Pt particles on Pt-Na/SiO$_2$ catalyst seems to adopt the disordered 2D raft-like structure, and no lattice fringe was observed. That is, Pt species still have the tendency toward agglomeration but not crystallization, which guaranteed higher atomic utilization

of Pt. From Fig. 3d, We deduced that the strong interaction between Pt and Na had prevented the nucleation of Pt crystals, leading to the formation of disordered clusters of Pt-O$_x$(OH)-Na species. Compared to Pt particles on Pt/SiO$_2$, the planar-distributed Pt-O$_x$(OH)-Na clusters would exhibit better atomic utilization, which also corresponds to the results of CO pulse chemisorption analysis. Additionally, more coordinatively unsaturated sites would be formed on Pt-Na/SiO$_2$ compared to the solid nanoparticles formed on Pt/SiO$_2$, which should be beneficial to HCHO oxidation reaction.

Previously, atomically dispersed Pt-O$_x$(OH)-Na was considered to be the active site in HCHO oxidation [10,17]; nevertheless, it has also been argued that a volcano-like relationship exists between the reaction rates and platinum size, on the scale of single-atoms, nanoclusters and nanoparticles [39]. Namely, Pt nanoclusters have the best performance in HCHO oxidation. In this study, both Pt-O$_x$(OH)-Na and Pt-O$_x$(OH)-Na atomically dispersed clusters could be observed on the Pt-Na/SiO$_2$ catalyst, which might explain its superior activity in HCHO oxidation. To further verify the difference in states of Pt species on Pt/SiO$_2$ and Pt-Na/SiO$_2$ samples, we further performed the *in situ* DRIFTS experiments of CO adsorption (as shown in Fig. 4). Based on the result of STEM, for Pt/SiO$_2$ catalyst, the peak at 2098 cm^{-1} could be assigned to CO linearly adsorbed on the terraces of Pt nanoparticles, while the peak
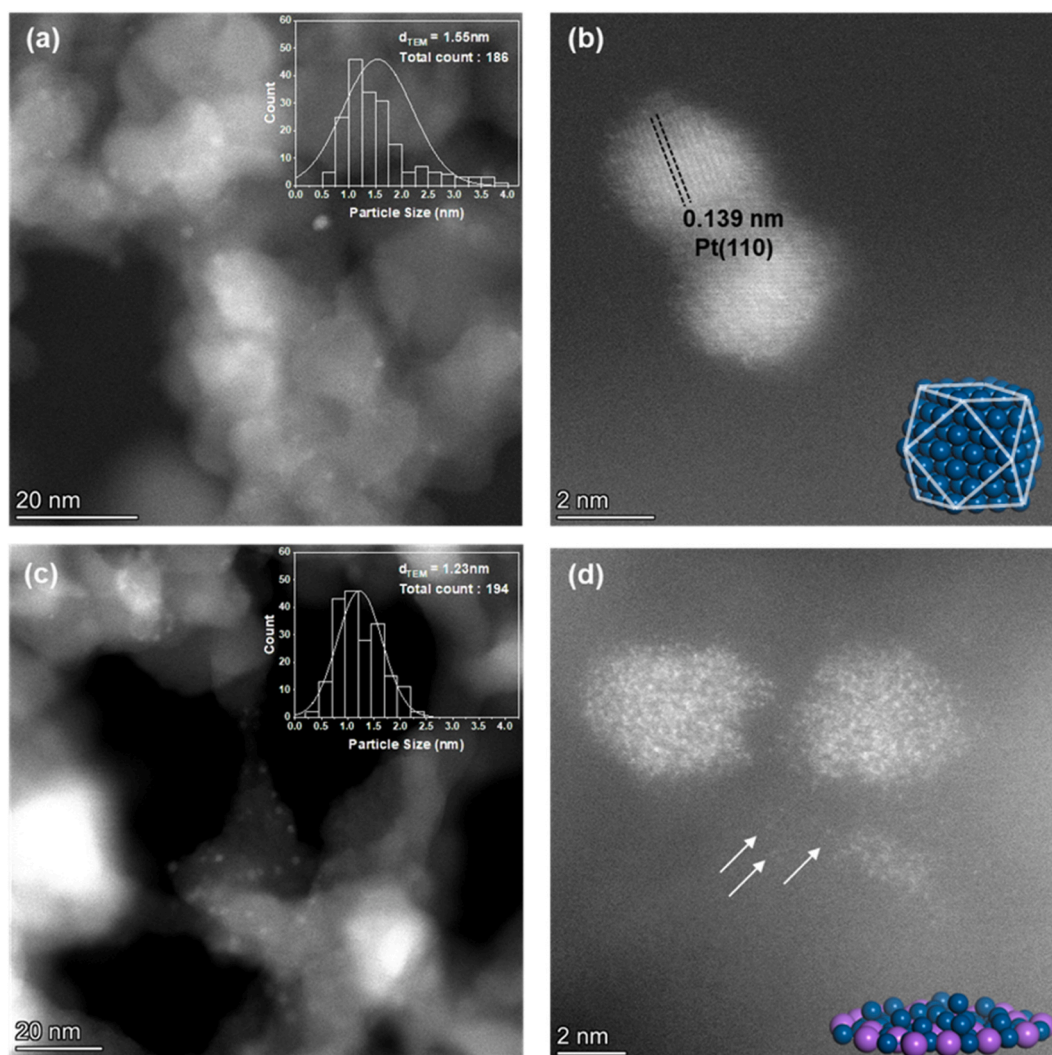
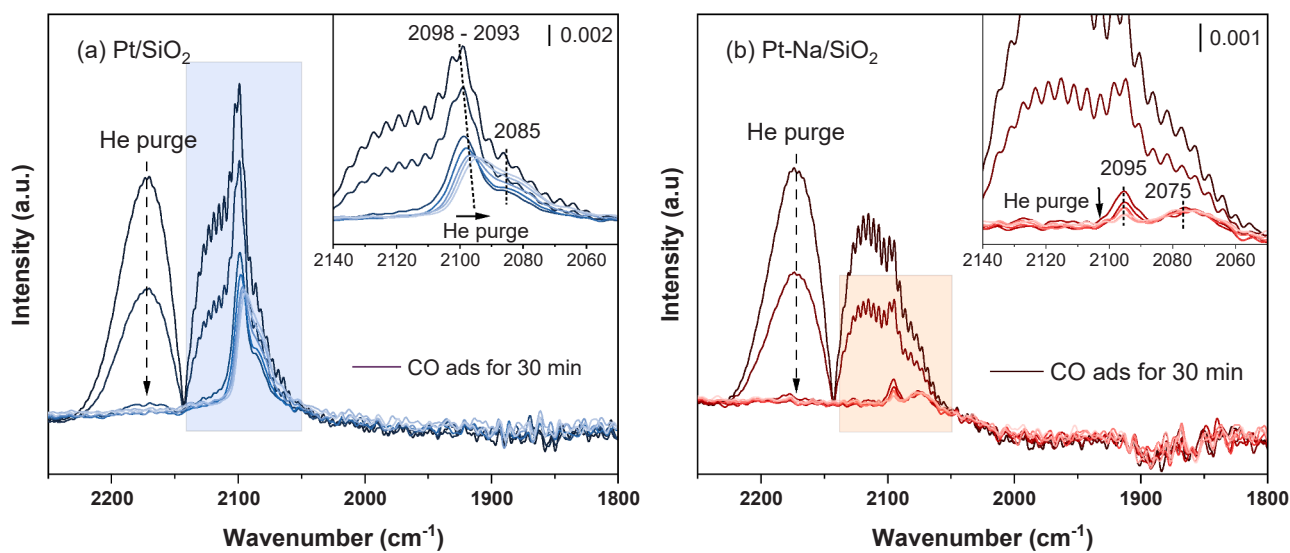**Fig. 3.** HAADF-STEM images with Pt particle distribution of (a-b) Pt/SiO$_2$ and (c-d) Pt-Na/SiO$_2$ samples.

Fig. 4. *In situ* DRIFTS results of CO adsorption over (a) Pt/SiO$_2$ and (b) Pt-Na/SiO$_2$。.

at 2085 cm^{-1} could be ascribed to CO adsorbed on the steps [40–43]. When it was purged by He flow, it is worth noting that a red shift was observed for the IR peaks during CO desorption, which was correlated with changes in dipole-dipole coupling between CO molecules on the Pt terrace, which is a typical feature of CO adsorption sites on Pt nanoparticles [44]. On Pt-Na/SiO$_2$, the peak at 2095 cm^{-1} was assigned to CO adsorbed on atomically dispersed Pt-O$_x$(OH)-Na, while the peak at 2075 cm^{-1} was ascribed to CO adsorbed on Pt-O$_x$(OH)-Na nanocluster species [43]. Differently, there was no red shift but only a decrease in the intensity of peaks during CO desorption, indicating the existence of smaller clusters.

3.4.3. Surface hydroxyls

According to the following mechanism: $2CO + 2OH \rightarrow 2CO_2 + H_2$, CO molecules were used as a probe to investigate OH species on the surface of the catalysts, and the results can be seen in Fig. 5. It is well known that the surface of SiO$_2$ is hydroxylated; however, the OH groups on pure SiO$_2$ are rather inert, for the peaks of Si-OH did not appear until 600 °C. After Pt loading on the SiO$_2$ support, a newly emerging peak starting at 440 °C could be attributed to Pt-OH [45]. Meanwhile, the intensity of Si-OH was greatly enhanced, suggesting the promotion effect of Pt in activating part of the Si-OH. Further, after Na doping, the peak of Pt-OH moved down to 250 °C, and the intensity increased significantly as well, suggesting that the formation of Pt-O$_x$(OH)-Na species enhanced the activation of OH groups. Some previous works have reported that OH groups on supports, i.e., Ti-OH and Al-OH [17, 46], would participate the decomposition of HCHO, but it was also argued that the active OH groups are only associated with Pt, which are independent from the OH of the support. Hence, the function of the different types of OH needs to be further explored.

3.5. Reaction mechanism

The reaction mechanisms of HCHO oxidation on Pt/SiO$_2$ and Pt-Na/SiO$_2$ were investigated by *in situ* DRIFTS at ambient temperature. For comparison, HCHO adsorption on the SiO$_2$ support was also studied, and the results are shown in Fig. S6. When the SiO$_2$ support was exposed to a flow of HCHO + He, very weak peaks at 3720–3740 cm^{-1} (negative) and 2750–3000 cm^{-1} were observed. The first one is assigned to the consumption of Si-OH, and the latter one is ascribed to ν(C-H) [47]. Unlike on the traditional supports TiO$_2$ or Al$_2$O$_3$, no intermediates from further transformation (DOM, formate, etc.) were observed on SiO$_2$, indicating that the interaction between HCHO molecules and the SiO$_2$

support was merely physisorption based on van der Waals forces. Hence, we may conclude that the OH species on this SiO$_2$ support were too inert to participate in the reaction, which was in accordance with the CO-TPR results.

For Pt/SiO$_2$ (Fig. 6a), on exposure to the flow of HCHO + He, only CO linearly adsorbed on Pt was observed (2090 cm^{-1}), which is a very rare phenomenon [48]. According to our previous work, on Pt/TiO$_2$ catalysts, HCHO tends to adsorb on the support and further transform into DOM and formate species via Ti-OH. However, in this work, for the Pt/SiO$_2$ catalyst, the chemisorption and transformation of HCHO on the SiO$_2$ support was negligible; hence, the only adsorption site for HCHO was on Pt sites. Due to the lack of active OH species, dehydrogenation of HCHO was likely to form the intermediate CO on the Pt sites. On the introduction of O$_2$, it was further oxidized to form CO$_2$. We further inlet HCHO + O$_2$ + H$_2$O + He (Fig. S7), and still no sign of formate species could be observed. Hence, on Pt/SiO$_2$, we have gained further insight into the mechanism of HCHO oxidation, as shown in Scheme 1. In the past, we considered the reaction mechanism as a bifurcated tree with the bifurcation node at the formate species; afterward, HCOO could be either decomposed into CO or directly oxidized into the final product of CO$_2$, whereas here we discovered that the formation of CO might be parallel to that of formate species, and derive directly from HCHO.

On the other hand, on Pt-Na/SiO$_2$ (Fig. 6b), since the active Pt-O$_x$(OH)-Na species were formed, formate species (1600 cm^{-1} and 1350 cm^{-1}) were formed after the introduction of HCHO [48]. This suggests the OH in Pt-O$_x$(OH)-Na was active in contributing to HCHO adsorption and further transformation. And as previously mentioned, formate species are the key to determining the reaction rate and would likely accumulate on the catalyst. The formate species degraded a bit during He and O$_2$ + He purging (33.5%, as calculated in Table S3), while with the introduction of H$_2$O and O$_2$ together, the accumulated formate species disappeared and fully converted into CO$_2$ and H$_2$O. In order to prevent overlap between peaks for formate species and δ(H$_2$O) (1650 cm^{-1}), He purge was conducted in the final stage. It could be observed that both formate and water species have completely disappeared, which proves that the co-introduction of H$_2$O and O$_2$ would lead to the degradation of formate species. It is worth noting that different from on the case Pt/TiO$_2$, there was no dioxymethylene (DOM) observed in the whole process, which may due to the activity of OH species in Pt-O$_x$(OH)-Na being higher than Ti-OH species, leading to instantaneous decomposition of the metastable DOM.

To further prove our assumptions, DFT calculations were applied to identify the different pathways, and a Pt terrace was built to simulate the
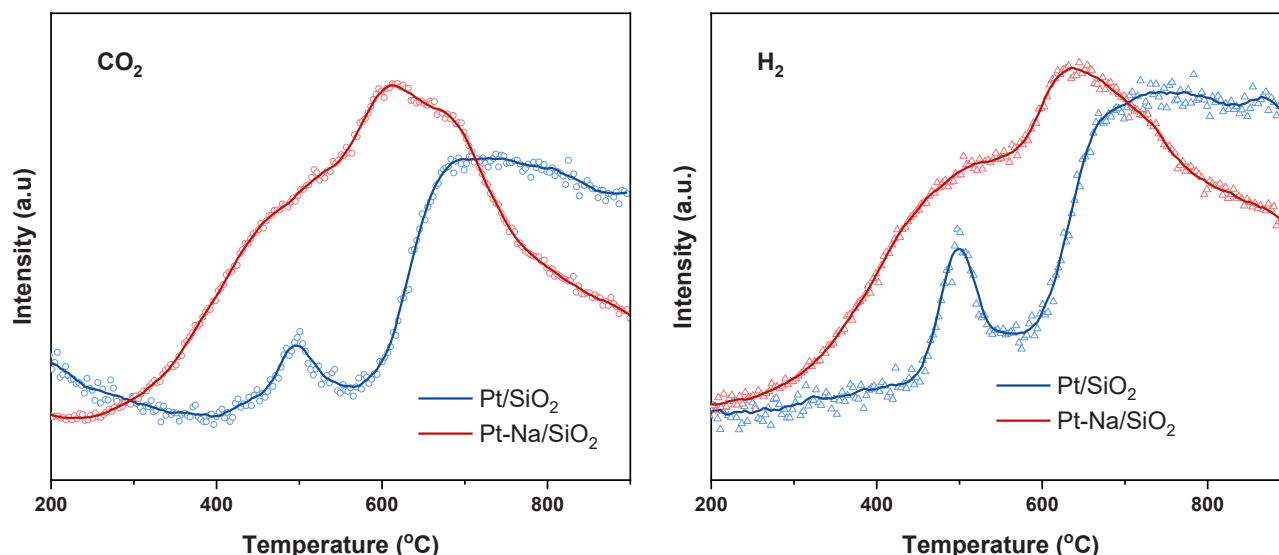

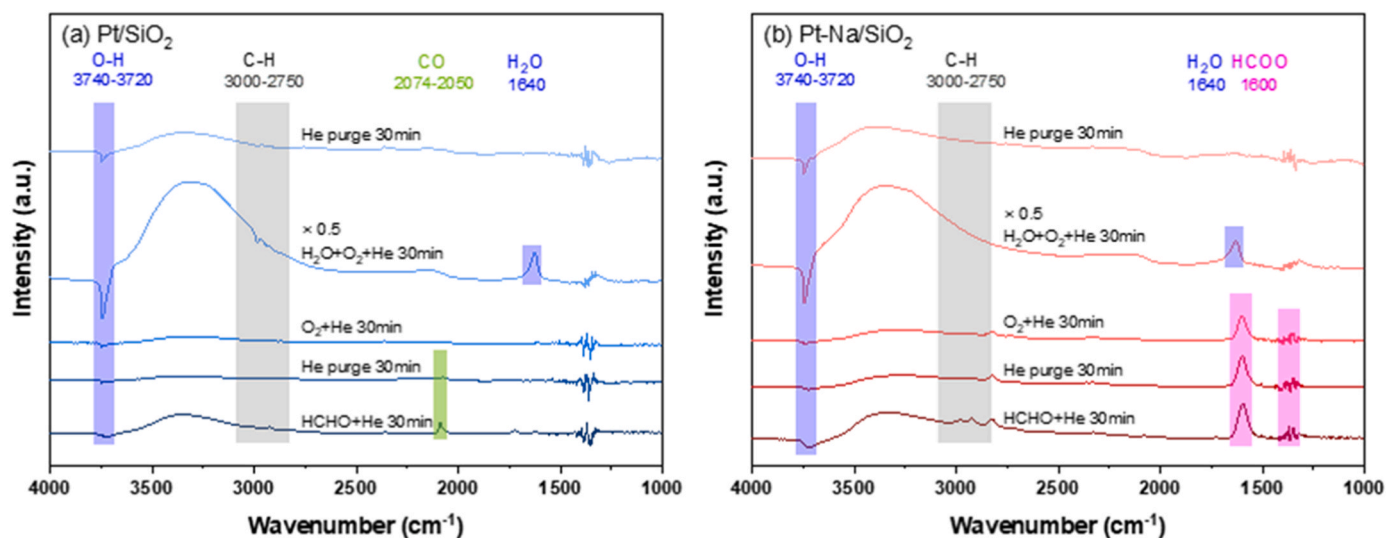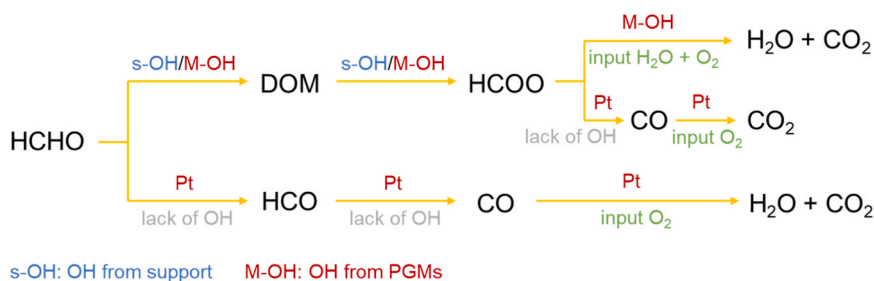**Fig. 5.** CO-TPR for Pt/SiO$_2$ and Pt-Na/SiO$_2$.

Fig. 6. Steady-state *in situ* DRIFTS spectra over (a) Pt/SiO$_2$ and (b) Pt-Na/SiO$_2$, in a gas flow of (1) HCHO +He for 60 min, followed by (2) He purging for 60 min, then (3) O$_2$ + He for 60 min, finally by (4) O$_2$ + H$_2$O + He for 60 min at room temperature. Reaction conditions: 120 ppm HCHO, 35% RH, 20% O$_2$, He balance, total flow rate of 100 mL/min.

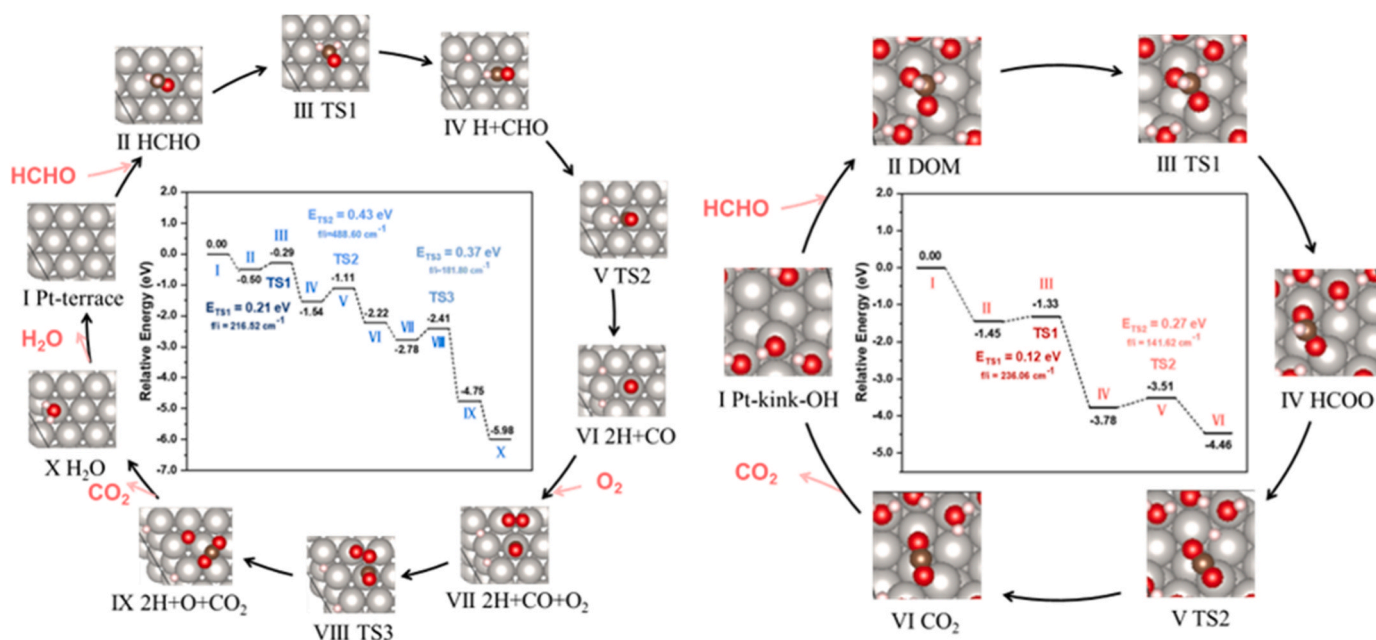**Scheme 1.** Reaction pathway of HCHO oxidation process.

Fig. 7. The calculation processes for the dehydrogenation of HCHO on (a) Pt terrace, and HCHO transformation with OH participation on (b) hydroxylated Pt slab with coordinatively unsaturated Pt sites. Red, white, brown, grey balls denote as O, H, C, Pt respectively.

Pt nanoparticles (Fig. S8). As shown in Fig. 7a, when an HCHO molecule approached the slab, exothermic adsorption occurred, with an adsorption energy of -0.50 eV. The O atom, as the most electronegative element in HCHO, was attached to the top site of Pt. When the first H was extracted from HCHO, the most stable adsorption site for H was at the three-fold site, i.e. FCC or HCP, while the adsorption form of HCO was changed into C-bonding. This process was exothermic, with an energy barrier of 0.21 eV. Then, the second H was extracted, leaving the CO molecule linearly attached to the top site of Pt, which was in accordance with the *in situ* DRIFTS spectra, and the energy barrier of this process was 0.43 eV. The above two processes should be considered to be first-order reactions, and the reaction rate (k) and half-life period ($t_{1/2}$) results based on the energy barriers are presented in Table S4. It is clear that the process of HCHO dehydrogenation on Pt is feasible, both thermodynamically and kinetically. With the introduction of O_2, CO and H could be further oxidized into CO_2 and H_2O, and the maximum energy barrier of the whole process was 0.43 eV.

For Pt-Na/SiO$_2$, we constructed a Pt kink with OH at the edge to simulate the coordinately unsaturated sites with active OH. When a HCHO molecule was near the slab, its adsorption and transformation took place simultaneously, and the DOM was formed after the geometry optimization. With the help of OH, DOM could be easily transformed to formate species and then CO_2 with a maximum energy barrier of 0.27 eV (Fig. 7b). Clearly, the active OH species could help to capture HCHO molecules to further facilitate the HCHO oxidation process. For supplementing OH, as shown in Fig. S9, H_2O and O_2 could be activated into Pt-OH with energy barrier of 0.05 eV.

Combining the results of DFT calculation with *in situ* DRIFTS, the HCHO oxidation pathway on Pt/SiO$_2$ is as follows:

$$HCHO \rightarrow CHO + H \tag{1}$$

$$CHO + H \rightarrow CO + 2H \tag{2}$$
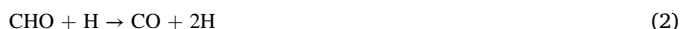
when O_2 is introduced in:

$$O_2 \rightarrow 2O \tag{3}$$

$$O + CO \rightarrow CO_2 \tag{4}$$

$$O + 2H \rightarrow H_2O \tag{5}$$

while on Pt-Na/SiO$_2$, the process is as follows:

$$HCHO + 2OH \rightarrow H_2COO + H_2O \tag{6}$$

$$H_2COO + OH \rightarrow HCOO + H_2O \tag{7}$$

$$HCOO + OH \rightarrow CO_2 + H_2O \tag{8}$$

when H_2O and O_2 is introduced in:

$$2H_2O + O_2 \rightarrow 4OH \tag{9}$$

4. Conclusion

In summary, Pt/SiO$_2$ catalyst exhibited superior activity compared to the traditional Pt/TiO$_2$ catalyst at the extremely low Pt loading of 0.05%, and the addition of Na endowed the Pt-Na/SiO$_2$ catalyst with outstanding catalytic activity, with complete elimination of 120 ppm HCHO at WHSV of 200,000 mL/(g_{cat}·h). Compared to Pt/TiO$_2$ with the SMSI, the EMSI existed between Pt and the SiO$_2$ support, which would lead to the *d*-band center of Pt moving closer to the Fermi level, as well as charge accumulation on Pt^0 species. Consequently, the adsorption and activation process of O_2 was facilitated, further promoting the degradation of HCHO. The addition of Na impacts the process in three ways, including electron transfer from Na to Pt, enhancement of Pt dispersion, and incrementing active OH via the formation of Pt-O$_x$(OH)-Na species. Combining the results of experiments with DFT calculations, we

speculated that the change in Pt species also altered the reaction pathway; that is, sufficient OH would participate in HCHO adsorption and oxidation, otherwise dehydrogenation would occur on the Pt surface. In conclusion, with SiO$_2$ as the support and Na as the promoter, the Pt-Na/SiO$_2$ catalyst has shown great potential for practical application.

CRediT authorship contribution statement

Liu Xiaofeng: Validation, Formal analysis, Data curation. **Chen Xudong:** Validation, Formal analysis, Data curation. **Wang Chunying:** Validation, Investigation, Data curation. **He Guangzhi:** Writing – review & editing, Visualization, Software. **Wang Jingyi:** Writing – original draft, Investigation, Formal analysis, Data curation. **He Hong:** Writing – review & editing, Supervision, Resources, Project administration, Conceptualization. **Shan Wenpo:** Validation, Methodology, Funding acquisition, Conceptualization. **Li Yaobin:** Writing – review & editing, Methodology, Conceptualization.

Declaration of Competing Interest

The authors declare that they have no known competing financial interests or personal relationships that could have appeared to influence the work reported in this paper.

Data availability

Data will be made available on request.

Acknowledgements

Appendix A. Supporting information

Supplementary data associated with this article can be found in the online version at doi:10.1016/j.apcatb.2024.123787.

References

[1] W.H. Liang, X.D. Yang, Indoor formaldehyde in real buildings: emission source identification, overall emission rate estimation, concentration increase and decay patterns, Build. Environ. 69 (2013) 114–120.

[2] S. Suresh, T.J. Bandosz, Removal of formaldehyde on carbon -based materials: a review of the recent approaches and findings, Carbon 137 (2018) 207–221.

[3] C. He, J. Cheng, X. Zhang, M. Douthwaite, S. Pattisson, Z. Hao, Recent advances in the catalytic oxidation of volatile organic compounds: a review based on pollutant sorts and sources, Chem. Rev. 119 (2019) 4471–4568.

[4] C. Wang, Y. Li, C. Zhang, X. Chen, C. Liu, W. Weng, W. Shan, H. He, A simple strategy to improve Pd dispersion and enhance Pd/TiO$_2$ catalytic activity for formaldehyde oxidation: the roles of surface defects, Appl. Catal. B 282 (2021).

[5] L. Nie, J. Yu, M. Jaroniec, F.F. Tao, Room-temperature catalytic oxidation of formaldehyde on catalysts, Catal. Sci. Technol. 6 (2016) 3649–3669.

[6] J. Guo, C. Lin, C. Jiang, P. Zhang, Review on noble metal-based catalysts for formaldehyde oxidation at room temperature, Appl. Surf. Sci. 475 (2019) 237–255.

[7] L. Miao, J.L. Wang, P.Y. Zhang, Review on manganese dioxide for catalytic oxidation of airborne formaldehyde, Appl. Surf. Sci. 466 (2019) 441–453.

[8] C.B. Zhang, H. He, A comparative study of TiO$_2$ supported noble metal catalysts for the oxidation of formaldehyde at room temperature, Catal. Today 126 (2007) 345–350.

[9] S. Colussi, M. Boaro, L. de Rogatis, A. Pappacena, C. de Leitenburg, J. Llorca, A. Trovarelli, Room temperature oxidation of formaldehyde on Pt-based catalysts: a comparison between ceria and other supports (TiO$_2$, Al$_2$O$_3$ and ZrO$_2$), Catal. Today 253 (2015) 163–171.

[10] C.B. Zhang, F.D. Liu, Y.P. Zhai, H. Ariga, N. Yi, Y.C. Liu, K. Asakura, M. Flytzani-Stephanopoulos, H. He, Alkali-metal-promoted Pt/TiO$_2$ opens a more efficient pathway to formaldehyde oxidation at ambient temperatures, Angew. Chem. Int. Ed. 51 (2012) 9628–9632.

[11] J. Zhang, X. Qin, X. Chu, M. Chen, X. Chen, J. Chen, H. He, C. Zhang, Tuning metal-support interaction of Pt-CeO₂ catalysts for enhanced oxidation reactivity, Environ. Sci. Technol. 55 (2021) 16687–16698.

[12] M. He, Y. Cao, J. Ji, K. Li, H. Huang, Superior catalytic performance of Pd-loaded oxygen-vacancy-rich TiO₂ for formaldehyde oxidation at room temperature, J. Catal. 396 (2021) 122–135.

[13] X. Wang, X. Zou, Z. Rui, Y. Wang, H. Ji, Highly dispersed and active Pd nanoparticles over titania support through engineering oxygen vacancies and their anchoring effect, AIChE J. 66 (2020) e16288.

[14] Y. Li, C. Wang, C. Zhang, H. He, Formaldehyde oxidation on Pd/TiO₂ catalysts at room temperature: the effects of surface oxygen vacancies, Top. Catal. 63 (2020) 810–816.

[15] X. Qin, M. Chen, X. Chen, J. Zhang, X. Wang, J. Fang, C. Zhang, Effects of the metal–support interaction in Ru/CeO₂ nanostructures on active oxygen species for HCHO/CO oxidation, ACS Appl. Nano Mater. 5 (2022) 15574–15582.

[16] Z. Guo, X. Zhao, G. Chen, Z. Yang, T. Liu, R. Hu, X. Jiang, Activating Pt clusters for efficient removal of HCHO by modulating V^{n+} within V_xO_y support, Appl. Catal. B 333 (2023).

[17] Z. Zhang, G. He, Y. Li, C. Zhang, J. Ma, H. He, Effect of hydroxyl groups on metal anchoring and formaldehyde oxidation performance of Pt/Al₂O₃, Environ. Sci. Technol. 56 (2022) 10916–10924.

[18] C. Wang, Y. Li, L. Zheng, C. Zhang, Y. Wang, W. Shan, F. Liu, H. He, A. Nonoxide, Catalyst system study: alkali metal-promoted Pt/AC catalyst for formaldehyde oxidation at ambient temperature, ACS Catal. 11 (2020) 456–465.

[19] L. Zhang, Y. Jiang, B.-B. Chen, C. Shi, Y. Li, C. Wang, S. Han, S. Pan, L. Wang, X. Meng, F.-S. Xiao, Exceptional activity for formaldehyde combustion using siliceous Beta zeolite as a catalyst support, Catal. Today (2019).

[20] H. Zhao, B. Tang, J. Tang, Y. Cai, Y. Cui, H. Liu, L. Wang, Y. Wang, W. Zhan, Y. Guo, Y. Guo, Ambient temperature formaldehyde oxidation on the Pt/Na-ZSM-5 catalyst: tuning adsorption capacity and the Pt chemical state, Ind. Eng. Chem. Res. 60 (2021) 7132–7144.

[21] S. Chen, S. Gueddida, M. Badawi, S. Lebègue, J.-M. Giraudon, J. Dhainaut, S. Royer, J.-F. Lamonier, Unravelling the critical role of silanol in Pt/SiO₂ for room temperature HCHO oxidation: an experimental and DFT study, Appl. Catal. B 331 (2023).

[22] X. Ding, D. He, S. Li, Y. Liang, J. Dai, P. Yao, M. Zhao, J. Wang, Y. Chen, Enhancing Pt anti-sintering and oxidation-resistance by bifunctional silica overcoating for the long-term NO oxidation stability, Appl. Catal. A 647 (2022).

[23] Z. Zheng, X. Wang, J. Liu, J. Xiao, Z. Hu, Si doping influence on the catalytic performance of Pt/TiO₂ mesoporous film catalyst for low-temperature methanol combustion, Appl. Surf. Sci. 309 (2014) 144–152.

[24] E. Jimenez-Izal, H. Zhai, J.-Y. Liu, A.N. Alexandrova, Nanoalloying MgO-deposited Pt clusters with Si To control the selectivity of alkane dehydrogenation, ACS Catal. 8 (2018) 8346–8356.

[25] D. Chen, Z. Pu, P. Wang, R. Lu, W. Zeng, D. Wu, Y. Yao, J. Zhu, J. Yu, P. Ji, S. Mu, Mapping hydrogen evolution activity trends of intermetallic Pt-group silicides, ACS Catal. 12 (2022) 2623–2631.

[26] T. Dong, J. Ji, L. Yu, P. Huang, Y. Li, Z. Suo, B. Liu, Z. Hu, H. Huang, Tunable interfacial electronic Pd-Si interaction boosts catalysis via accelerating O₂ and H₂O activation, JACS Au 3 (2023) 1230–1240.

[27] Y. Zhai, D. Pierre, R. Si, W. Deng, P. Ferrin, A.U. Nilekar, G. Peng, J.A. Herron, D. C. Bell, H. Saltsburg, M. Mavrikakis, M. Flytzani-Stephanopoulos, Alkali-stabilized Pt-OH species catalyze low-temperature water-gas shift reactions, Science 329 (2010) 1633.

[28] J.H. Pazmiño, M. Shekhar, W. Damion Williams, M. Cem Akatay, J.T. Miller, W. Nicholas Delgass, F.H. Ribeiro, Metallic Pt as active sites for the water–gas shift reaction on alkali-promoted supported catalysts, J. Catal. 286 (2012) 279–286.

[29] X.L. Zhu, M. Shen, L.L. Lobban, R.G. Mallinson, Structural effects of Na promotion for high water gas shift activity on Pt–Na/TiO₂, J. Catal. 278 (2011) 123–132.

[30] Z.F. Bai, B.B. Chen, Q. Zhao, C. Shi, M. Crocker, Positive effects of K^+ in hybrid CoMn-K and Pd/Ba/Al₂O₃ catalysts for NOₓ storage and reduction, Appl. Catal. B 249 (2019) 333–345.

[31] J. Wang, J. Li, P. Zhang, G. Zhang, Understanding the "seesaw effect" of interlayered K^+ with different structure in manganese oxides for the enhanced formaldehyde oxidation, Appl. Catal. B 224 (2018) 863–870.

[32] Y.B. Li, X.Y. Chen, C.Y. Wang, C.B. Zhang, H. He, Sodium enhances Ir/TiO₂ activity for catalytic oxidation of formaldehyde at ambient temperature, ACS Catal. 8 (2018) 11377–11385.

[33] C.B. Zhang, Y.B. Li, Y.F. Wang, H. He, Sodium-promoted Pd/TiO₂ for catalytic oxidation of formaldehyde at ambient temperature, Environ. Sci. Technol. 48 (2014) 5816–5822.

[34] J.H. Kwak, J. Hu, D. Mei, C.W. Yi, D.H. Kim, C. Peden, Coordinatively unsaturated Al^{3+} centers as binding sites for active catalyst phases of platinum on Platinum on γ-Al₂O₃, Science 325 (2009) 1670–1673.

[35] B. Hammer, J.K. Nørskov, Why gold is the noblest of all the metals, Nature 376 (1995) 238–240.

[36] J.K. Nørskov, Electronic factors in catalysis, Prog. Surf. Sci. 38 (1991) 103–144.

[37] J.K. Nørskov, Chemisorption on metal surfaces, Rep. Prog. Phys. 53 (1999) 1253–1295.

[38] S. Wang, Y. Wang, F. Wang, Room temperature HCHO oxidation over the Pt/CeO₂ catalysts with different oxygen mobilities by changing ceria shapes, Appl. Catal. A 630 (2022).

[39] X. Sun, J. Lin, Y. Chen, Y. Wang, L. Li, S. Miao, X. Pan, X. Wang, Unravelling platinum nanoclusters as active sites to lower the catalyst loading for formaldehyde oxidation, Commun. Chem. 2 (2019).

[40] L. Li, L. Li, L. Wang, X. Zhao, Z. Hua, Y. Chen, X. Li, X. Gu, Enhanced catalytic decomposition of formaldehyde in low temperature and dry environment over silicate-decorated titania supported sodium-stabilized platinum catalyst, Appl. Catal. B (2020).

[41] J. Chen, M. Jiang, W. Xua, J. Chen, Z. Hong, H. Jia, Incorporating Mn cation as anchor to atomically disperse Pt on TiO₂ for lowtemperature removal of formaldehyde, Appl. Catal. B 259 (2019).

[42] L. Zhu, J. Wang, S. Rong, H. Wang, P. Zhang, Cerium modified birnessite-type MnO₂ for gaseous formaldehyde oxidation at low temperature, Appl, Catal. B 211 (2017) 212–221.

[43] Utilizing quantitative in situ FTIR spectroscopy to identify wellcoordinated Pt atoms as the active site for CO oxidation on Al2O3-supported Pt catalysts, ACS Catal., 6 (2016) 5599–5609.

[44] K. Ding, A. Gulec, A.M. Johnson, N.M. Schweitzer, G.D. Stucky, L.D. Marks, P. C. Stair, Identification of active sites in CO oxidation and water-gas shift over supported Pt catalysts, Science 350 (2015) 189–192.

[45] Y. Chen, Y. Feng, L. Li, J. Liu, X. Pan, W. Liu, F. Wei, Y. Cui, B. Qiao, X. Sun, X. Li, J. Lin, S. Lin, X. Wang, T. Zhang, Identification of active sites on high-performance Pt/Al₂O₃ catalyst for cryogenic CO oxidation, ACS Catal. 10 (2020) 8815–8824.

[46] X. Chen, G. He, Y. Li, M. Chen, X. Qin, C. Zhang, H. He, Identification of a facile pathway for dioxymethylene conversion to formate catalyzed by surface hydroxyl on TiO2-based catalyst, ACS Catal. 10 (2020) 9706–9715.

[47] X. Chen, G. He, Y. Li, M. Chen, X. Qin, C. Zhang, H. He, Identification of a facile pathway for dioxymethylene conversion to formate catalyzed by surface hydroxyl on TiO₂-based catalyst, ACS Catal. 10 (2020) 9706–9715.

[48] C. Zhang, H. He, K.-i Tanaka, Catalytic performance and mechanism of a Pt/TiO₂ catalyst for the oxidation of formaldehyde at room temperature, Appl. Catal. B 65 (2006) 37–43.